

Large-Scale Fixed-Wing UAV Swarm System Control With Collision Avoidance and Formation Maneuver

Jiacheng Li , Yangwang Fang , Haoyun Cheng, Zhikai Wang , Zihao Wu , and Mengjie Zeng

Abstract—In this article, a distributed control algorithm for a large-scale fixed-wing unmanned aerial vehicle (UAV) swarm system of collision avoidance and formation maneuver is proposed, which can meet the demands of a dense swarm with collaborative autonomy. First, a novel structure of a swarm is introduced, which can provide the reserved maneuverable space for UAVs during the flight. Besides, inspired by the movement of bird flocks, the light transmission model is proposed to improve the conventional potential field functions, which can realize the UAV swarm with the capability of repulsion in the short-range, speed and position cooperation in the middle range, and attraction in the remote range. Then, the distributed control architecture and the control algorithm of UAVs are designed, and the stability of the swarm is proved correspondingly. In the end, several numerical simulation results show the effectiveness and superiority of the proposed method, which illustrates the distributed control architecture of the swarm system to be more adaptable, stable, and scalable. Therefore, the proposed control algorithm provides strong theoretical support for the actual application in a large-scale fixed-wing UAV swarm system collaborative autonomy.

Index Terms—Collision avoidance, large-scale, potential field functions, swarm system, unmanned aerial vehicle (UAV).

I. INTRODUCTION

IN RECENT years, there has been a surge of interest among multi-unmanned aerial vehicles (UAVs), which have wide applications in civilian and military. Compared with the single-UAV, the multi-UAVs are more capable, covering a larger area and completing more tasks with less cost, higher flexibility, and stronger robustness [1]. Among them, the key issue for the multi-UAV system study is to coordinate the obstacle avoidance and collision avoidance between UAVs [2].

There have been extensive studies of obstacle avoidance methods for multi-UAV, including mathematical planning, graph theory, spatial decomposition, intelligent algorithm, random

Manuscript received 28 September 2021; revised 11 August 2022; accepted 29 September 2022. This work was supported by the National Natural Science Foundation of China under Grant 61973253, Grant 62006192, and Grant 62273283. (*Corresponding author: Yangwang Fang*.)

Jiacheng Li, Yangwang Fang, and Haoyun Cheng are with the Unmanned System Research Institute, Northwestern Polytechnical University, Xian 710072, China (e-mail: jiacheng_li@mail.nwpu.edu.cn; ywfang@nwpu.edu.cn; cheng_haoyu@nwpu.edu.cn).

Zhikai Wang is with the School of Aerospace, Northwestern Polytechnical University, Xian 710072, China (e-mail: zhikaiwang01@163.com).

Zihao Wu is with the School of Automation Science and Electrical Engineering, Beihang University, Beijing 100191, China (e-mail: wulaoker47@163.com).

Mengjie Zeng is with the College of Energy and Power Engineering, Nanjing University of Aeronautics and Astronautics, Nanjing 210016, China (e-mail: mjjzeng@nuaa.edu.cn).

Digital Object Identifier 10.1109/JST.2022.3212068

planning, machine learning, and potential field function [3], [4]. In completing complex tasks, dynamic switching of formations is required. Therefore, it is not enough to rely solely on obstacle avoidance methods [5], [6]. It can be said that the coordinated control of multi-UAV not only relies on obstacle avoidance methods but also requires formation control as the basis. Virtual structure [7], behavior-based [8], and leader following [9] are common formations studied in recent years. With the combination of the above methods, many effective applications have been achieved in multi-UAV control. Yan [10] reported an approach combining virtual structure with artificial potential field (APF), which realized a high accuracy of formation keeping and transforming. Yang proposed a formation control method with collision, obstacle avoidance, and connectivity maintenance based on neural-network by the combination of the APF method and leader following structure [11]. It can be seen from the existing literature that the common methods had good control effects in the formation and obstacle avoidance control of a certain number of the multi-UAV.

With the requirements of practical applications, demands for the number of UAVs in the multi-UAV have also increased significantly, which gradually forms UAV swarm operation. The UAV swarm system can be considered as a form of collective behavior of a large number of interacting UAVs, which desire to achieve a common group goal. However, the computational complexity grows exponentially when the number of the UAVs increases continuously [12], especially in the large-scale UAV swarm system in which the number size of UAV is over hundreds [13], [14]. That is to say, the conventional formation and obstacle avoidance control methods are no longer suitable for such situations.

In the research of large-scale UAV swarm control field, it can be divided into two main research parts based on the autonomy degree of UAVs. One part is that many companies use UAVs in the light show, which is the automation systems devised for live performances that could control one to potentially thousands of UAVs [15], [16]. As yet, a Guinness World Record had been created by Intel because “The Most UAVs Airborne Simultaneously,” which has a swarm of 500 UAVs [17]. In addition, the largest UAV swarm had been developed by Ehang [18], whose experiment was more than 1000 UAVs. However, these UAV swarm control methods were just tracking the predefined paths with ensuring the safety and reliability of each UAV, which the whole swarm will be affected accordingly if there is a fault problem with any individual UAVs. Therefore, it is not satisfied that the criteria of collaborative autonomy were used in such a case. Besides, these control systems are often under a central control architecture that needs every UAV to communicate with the ground stations, which means a huge calculation amount and high hardware equipment requirements.

Another is that the collaborative autonomy UAV swarm with the characteristics of collision avoidance, path planning, and decision making autonomously [19], [20], [21]. But the scales of UAVs in their theoretical research are only about a hundred, whereas the numbers of UAVs in actual flying are only a few dozen. The military of the U.S. did an experiment called Perdix with fixed-wing drone swarms, which realized 103 autonomous UAVs adaptive formation flying. Vasarhelyi et al., [23] realized a swarm of 30 self-organized UAVs in field experiments, which was the first time reported in detail to achieve UAVs collaborative autonomy system in outdoor aerial with such number scale UAV swarm. Wang et al., [24] and Chen et al., [25] aimed at the formation control problem of large-scale fixed-wing UAV swarm with a multilayered group-based architecture and carried out the numerical simulation of the flying process with 100 fixed-wing UAVs swarm and realized that 21 UAVs were actually flying in field experiments, respectively. Chung [26] completed the cooperative autonomous actual flight with 50 fixed-wing UAVs in a low-cost and open-source component. Kushleyev [27] mentioned a useful control architecture and algorithms to coordinate a swarm of 20 quadrotors, which is at the expense of flexibility. Unfortunately, the proposed control mechanisms and structures have effective effects in UAV swarm control, but it is uncertain whether their system can still steady working when the scale of the swarm continues increasing.

Besides, stigmergy mechanism is widely adopted in swarm intelligence [28], [29], whose information exchanges are through the pheromone left in the environment by other agents. Ant colony algorithm is a typical one based on the stigmergy [30]. A swarm robot interaction strategy via radio frequency identification tags was proposed by Tang [31], which can carry out the dynamic target searching and tracking based on the stigmergy mechanism. However, this method is only suitable for cooperation between individuals without intelligence and cognitive simplification to complete complex tasks. In particular, the stigmergy must take time to continuously improve the information environment, which is not suitable for the UAV swarm with strict flight real-time requirements. Moreover, it is also difficult to realize the physical transfer between pheromones in the actual flight of UAV swarms, especially for the large-scale systems.

There were some research works based on multiagent theory [32], especially in solving large-scale communication problems [33]. But unlike multiagent under ideal model and quadrotors, fixed-wing UAVs have limited turn radius and minimum flight speed, which determine these have less maneuverable and more strictly flying constraints [34], [35]. Some researchers focused on machine learning to solve these problems, which suffer from the drawbacks including only theory feasible, unable to prove the converge of the algorithm, and, in addition, the requirement of high modeling accuracy with complicated calculation [36]. Therefore, it should be pointed out that a number of issues related to swarm control need to be resolved immediately. In particular, how to achieve cooperative control of large-scale swarm based on the suitable obstacle avoidance and formation control algorithms is still a challenge.

To solve this problem, a collision avoidance control method for large-scale fixed-wing UAV swarm based on formation reserved maneuvering space is proposed, which has the main contributions as follows.

- 1) The light transmission model (LTM) is added to the conventional potential field functions to ensure the UAV

flying decisions about collision avoidance by choosing the maneuvering space in a short time.

- 2) A novel swarm structure is proposed to reserve the maneuver space for UAVs obstacle avoidance and collision avoidance, which can make every UAV to detect sufficient light transmission. The capability of scalability and reconstruction for the swarm is improved under such structure, which ensures that only a small part of the swarm will be influenced rather than the whole one, when the swarm runs into obstacles or has a collision with each other.
- 3) A distributed control architecture that divides the large-scale swarm into groups by making full use of parallelism is proposed, which reduces the complexity of task planning and the demand of communication capabilities.

II. PRELIMINARIES AND MODELING

A. Problem Statement

This article mainly solves the obstacle avoidance control problem of large-scale UAV swarm. By using the LTM, the conventional APF method is improved to avoid obstacles. To prevent the collision between UAVs within the swarm, a desired formation with reserved space for UAV maneuvering is designed. In particular, the control objective of this article can be described as

$$\lim_{t \rightarrow \infty} J = \{J_{\psi^\alpha} + J_{\psi^\circ} + J_{\psi^r}\}_{\min} \quad (1)$$

where J is the total energy of the system; J_{ψ^α} , J_{ψ° , and J_{ψ^r} are the energy for collision avoidance between UAVs, the energy for UAVs to avoid obstacles, and the energy for UAVs to maintain formation, respectively. When $t \rightarrow \infty$ and J gets its minimum value, the optimal swarm control performance is achieved. At this point, the swarm formation maintains the ideal configuration, and the speeds of all UAVs are the same. The algorithm flow is given in Appendix A.

B. Structure of Swarm

To control a large number of fixed-wing UAV swarm, we divide the swarm into several groups. A reference point of the swarm structure is set to maintain the formation structure of the swarm. Inspired by the layout of the high-rise apartment building, where the capacity of the daylighting for each building in their design process is considered fully, a new formation structure for the swarm in Fig. 1 is proposed in this article.

The maneuver space for UAVs is reserved under this structure through a certain regular arrangement and combination of each group position, which can provide enough light transmission and obstacle avoidance space for UAVs. Considering the scalability of the swarm, space is reserved on the right side of each group to ensure a new group to join at any time.

The matrix $\Xi_{n \times m}$ is used to describe the structure of the swarm, which consists of a certain number of partitioned matrices B_{lk} . And $\Xi_{n \times m}$ can specifically be expressed as (2) shown at the bottom of the next page, where

$$n = n_1 + n_2 + \dots + n_a$$

$$m = m_1 + m_2 + \dots + m_b$$

$$B_{lk} = B_{lk(n_l \times m_k)} \quad (l = 1, \dots, a; k = 1, \dots, b). \quad (3)$$

Considering the reserved space of the swarm structure, the following elements in matrix $\Xi_{n \times m}$ are defined as the partitioned

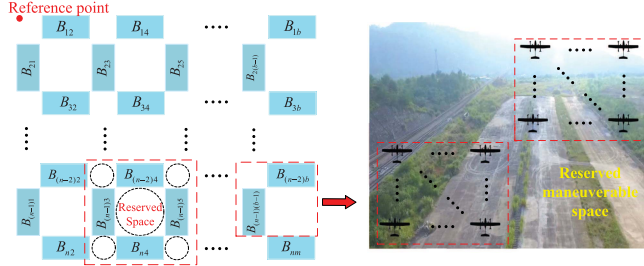


Fig. 1. Formation shape under ideal state.

matrices composed of 0.

$$\mathbf{B}_{lk} = \begin{cases} k = 1, 3, \dots, b-1, & l \text{ is odd} \\ k = 2, 4, \dots, b, & l \text{ is even} \end{cases} \quad (4)$$

In the matrix $\Xi_{n \times m}$, the elements of the partitioned matrix \mathbf{B}_{lk} are composed of each UAV element, which are specifically expressed as $\alpha_{ij}^{\mathbf{B}_{lk}} \in \mathbf{B}_{lk}$, where $\alpha_{ij}^{\mathbf{B}_{lk}}$ represents the UAV in the i th row and j th column of the group \mathbf{B}_{lk} and satisfies

$$\begin{cases} i = 1, \dots, n_1, & l = 1 \\ i = n_1 + \dots + n_{l-1} + 1, \dots, n_1 + \dots + n_{l-1} + n_l, & 1 < l \leq a \end{cases} \quad (5)$$

$$\begin{cases} j = 1, \dots, m_1, & k = 1 \\ j = m_1 + \dots + m_{k-1} + 1, \dots, m_1 + \dots + m_{k-1} + m_k, & 1 < k \leq b \end{cases} \quad (6)$$

For any UAV $\alpha_{ij}^{\mathbf{B}_{lk}}$, its coordinate position can be recorded as $\mathbf{q}_{ij}^{\mathbf{B}_{lk}} = [x_{ij}^{\mathbf{B}_{lk}}, y_{ij}^{\mathbf{B}_{lk}}]^T$. Assume that the coordinate space between every two UAVs is $\Delta \mathbf{q}_{ij}^{\mathbf{B}_{lk}} = [\Delta dx \quad \Delta dy]^T$. And we also define the coordinate of the element in the first row and first column of the structure matrix as the coordinate of reference point of the swarm structure, that is $\mathbf{q}^r = [0 \quad 0]^T$. Therefore, the relative position expression of the UAV $\alpha_{ij}^{\mathbf{B}_{lk}}$ is as

$$\mathbf{q}_{ij}^{\mathbf{B}_{lk}} - \mathbf{q}^r = \xi_{ij}^{\mathbf{B}_{lk}} \Delta \mathbf{q}_{ij}^{\mathbf{B}_{lk}} \quad (7)$$

where $\xi_{ij}^{\mathbf{B}_{lk}}$ is the coefficient matrix used to determine the distance between the reference point and UAV $\alpha_{ij}^{\mathbf{B}_{lk}}$ in the

swarm, which can be expressed as

$$\xi_{ij}^{\mathbf{B}_{lk}} = \begin{bmatrix} \xi_{ij1}^{\mathbf{B}_{lk}} & 0 \\ 0 & \xi_{ij2}^{\mathbf{B}_{lk}} \end{bmatrix} \quad (8)$$

where

$$\xi_{ij1}^{\mathbf{B}_{lk}} = \begin{cases} j-1, & l=1 \\ [(m_1 + \dots + m_{k-1}) + j] - 1, & 1 < l \leq a \end{cases} \quad (9)$$

$$\xi_{ij2}^{\mathbf{B}_{lk}} = \begin{cases} i-1, & k=1 \\ [(n_1 + \dots + n_{l-1}) + i] - 1, & 1 < k \leq b \end{cases} \quad (10)$$

C. Modeling of UAV

Suppose that the simplified dynamic model of UAV $\alpha_{ij}^{\mathbf{B}_{lk}}$ can be expressed as the following second-order integral system:

$$\begin{cases} \dot{\mathbf{q}}_{ij}^{\mathbf{B}_{lk}} = \mathbf{p}_{ij}^{\mathbf{B}_{lk}} \\ \dot{\mathbf{p}}_{ij}^{\mathbf{B}_{lk}} = \mathbf{u}_{ij}^{\mathbf{B}_{lk}} \end{cases} \quad (i=1, \dots, n_l; j=1, \dots, m_k) \quad (11)$$

where $\mathbf{p}_{ij}^{\mathbf{B}_{lk}}$ represents the speed of UAV $\alpha_{ij}^{\mathbf{B}_{lk}}$; $\mathbf{u}_{ij}^{\mathbf{B}_{lk}}$ is the system control input. It is worth noting that the process of constructing the UAV model can be found in Appendix B.

Considering the maneuverability of fixed-wing UAV, UAV $\alpha_{ij}^{\mathbf{B}_{lk}}$ should satisfy the following formula of constraint conditions:

$$\begin{cases} 0 < v_{\min}^{\mathbf{B}_{lk}} \leq v_{ij}^{\mathbf{B}_{lk}} \leq v_{\max}^{\mathbf{B}_{lk}} \\ |w_{ij}^{\mathbf{B}_{lk}}| \leq w_{\max}^{\mathbf{B}_{lk}} \\ R_t \geq R_{\min} \end{cases} \quad (12)$$

where $v_{\min}^{\mathbf{B}_{lk}}$ and $v_{\max}^{\mathbf{B}_{lk}}$ represent the minimum and maximum airspeed allowed by all UAVs in fixed altitude flight, respectively; $w_{ij}^{\mathbf{B}_{lk}}$ is the heading angular rate of UAV $\alpha_{ij}^{\mathbf{B}_{lk}}$; $w_{\max}^{\mathbf{B}_{lk}}$ is the maximum allowable heading angular rate of all UAVs; R_t is the turning radius of all UAVs; n_{\max} is the maximum overload of all UAVs, and the minimum turning radius can be expressed as

$$R_{\min} = \frac{(v_{ij}^{\mathbf{B}_{lk}})^2}{n_{\max}}. \quad (13)$$

$$\Xi_{n \times m} = \left[\begin{array}{ccccccccc} 0 & \cdots & 0 & \alpha_{1,m_1+1} & \cdots & \alpha_{1,m_1+m_2} & \cdots & \alpha_{1,m-m_b+1} & \cdots & \alpha_{1,m} \\ \vdots & \ddots & \vdots & \vdots & \ddots & \vdots & \ddots & \vdots & \ddots & \vdots & \vdots \\ 0 & \cdots & 0 & \alpha_{n_1,m_1+1} & \cdots & \alpha_{n_1,m_1+m_2} & \cdots & \alpha_{n_1,m-m_b+1} & \cdots & \alpha_{n_1,m} \\ \alpha_{n_1+1,1} & \cdots & \alpha_{n_1+1,m_1} & 0 & \cdots & 0 & \cdots & 0 & \cdots & 0 \\ \vdots & \ddots & \vdots & \vdots & \ddots & \vdots & \ddots & \vdots & \ddots & \vdots \\ \alpha_{n_1+n_2,1} & \cdots & \alpha_{n_1+n_2,m_1} & 0 & \cdots & 0 & \cdots & 0 & \cdots & 0 \\ \cdots & & \cdots & \cdots & & \cdots & \cdots & \cdots & & \cdots \\ \alpha_{n-n_a+1,1} & \cdots & \alpha_{n-n_a+1,m_1} & 0 & \cdots & 0 & \cdots & 0 & \cdots & 0 \\ \vdots & \ddots & \vdots & \vdots & \ddots & \vdots & \ddots & \vdots & \ddots & \vdots \\ \alpha_{n,1} & \cdots & \alpha_{n,m_1} & 0 & \cdots & 0 & \cdots & 0 & \cdots & 0 \end{array} \right] \quad (2)$$

D. Topology of Swarm

Let $\mathbf{G} = (\mathbf{v}, \varepsilon)$ represents a graph with n nodes, where $\mathbf{v} = \{v_1, v_2, \dots, v_n\}$ is the set of nodes and $\varepsilon \subseteq \mathbf{v} \times \mathbf{v}$ is the set of edges. Assuming that there is the information interaction between node ij and node pq , then there are edges that connect the two nodes. If $(ij, pq) \in \varepsilon \iff (pq, ij) \in \varepsilon$, the graph \mathbf{G} is called undirected. If there is a path between any two nodes, the undirected graph \mathbf{G} is called connected. Based on the definition of undirected graph, it can be known that any two connected nodes in the graph are bidirectional. To describe the relationship between nodes and edges, for an undirected graph \mathbf{G} with n nodes, we define the adjacency matrix $\mathbf{A} = [a_{ij,pq}] (i, j, p, q = 1, \dots, n)$ as

$$a_{ij,pq} = \begin{cases} 1, & (v_{ij}, v_{pq}) \in \varepsilon \\ 0, & \text{otherwise} \end{cases}. \quad (14)$$

\mathbf{L} is the Laplace matrix of graph \mathbf{G} , which can be defined as

$$\mathbf{L} = \mathbf{D} - \mathbf{A} \quad (15)$$

where \mathbf{D} is the degree matrix of graph \mathbf{G} .

In this article, the topology of the swarm is generated at time $t = 0$, which will remain unchanged when $t > 0$. The set of adjacent UAVs of UAV $\alpha_{ij}^{B_{lk}}$ at time $t = 0$ is defined as

$$N_{pq}^{\alpha B_{lk}}(t) = \left\{ \begin{array}{l} \left\| \mathbf{q}_{ij}^{\alpha B_{lk}} - \mathbf{q}_{pq}^{\alpha B_{lk}} \right\| < r_\alpha \\ (i, p = 1, \dots, n_l; j, q = 1, \dots, m_k) \end{array} \right\} \quad (16)$$

where $\|\cdot\|$ represents the Euclidean norm in \mathbb{R}^n ; $\mathbf{q}_{pq}^{\alpha B_{lk}}$ is the position of adjacent UAV $\alpha_{ij}^{B_{lk}}$; and r_α is the interaction radius of two UAVs in the same group.

To achieve large-scale swarm control and reduce communication costs, it is defined that members of the same group can communicate with each other. Namely, the UAVs in the partitioned matrix B_{lk} can communicate with each other, where other group members are treated as obstacles. Therefore, the set of obstacles detected by UAV $\alpha_{ij}^{B_{lk}}$ is time-varying. At time t , it can be expressed as

$$N_{ij}^o(t) = \left\{ \left\| \mathbf{q}_{ij}^{\alpha B_{lk}} - \mathbf{q}_\nu^o \right\| < r_o, \nu = 1, 2, \dots, N_o \right\} \quad (17)$$

where r_o is the repulsion radius of UAV $\alpha_{ij}^{B_{lk}}$ to obstacles; N_o is the number of obstacles; and \mathbf{q}_ν^o is the position of obstacles. Here, the obstacle set includes actual obstacles and nearby UAVs of other groups.

E. Light Transmission Model

Suppose that birds have an ability to feel the intensity of the light around themselves, i.e., they can feel strong light when there is no obstacle around. In this way, they can fly in a direction with less threat of collisions by judging the strength of light, and eventually form a stable distribution. Therefore, this property of the bird swarm is defined as LTM in this article [37].

We can also think that UAVs in the border and in the middle of the swarm have different abilities to feel the threat of collision, which is conducive to maintain the structure of the swarm. As the UAVs move closer to the middle of the swarm, the brightness that they feel is gradually getting weaken, and the light transmission is also getting weaken.

Considering the characteristics of fixed-wing UAVs that cannot fly backward in time, the field angle of any UAV is defined in $[-\frac{\pi}{3}, \frac{4\pi}{3}]$. Moreover, to simplify the calculation and improve the accuracy of the light transmission judgment, we divide the field of view evenly into five parts with $\frac{\pi}{3}$ as the interval, which

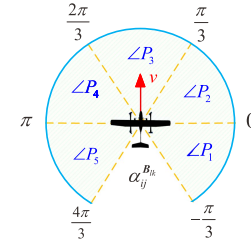


Fig. 2. LTM of UAV (Left).

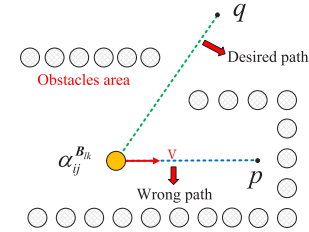


Fig. 3. Situation of partial transparency (Right).

is shown in Fig. 2. In the actual judgment process, the light transmission in each field angle is judged separately. Then, the field angle direction with the strongest light transmission will be selected for a UAV to fly. Especially, the field angle closest to the UAV speed direction will be selected to fly when there are multiple field angles with the same value of the light transmission. The light transmission can be considered as the probability of light transmission, that is, the probability of UAVs falling into the free space. Therefore, the candidate LTM can be defined as

$$P'(\alpha_{ij}^{B_{lk}}) = \frac{3A(\alpha_{ij}^{B_{lk}})}{5\pi} \quad (18)$$

where $A(\alpha_{ij}^{B_{lk}})$ is the angle of the selected field angle direction, which is the sum of the adjacent field angles with the same light transmission and can be expressed as

$$A(\alpha_{ij}^{B_{lk}}) = \dots + \angle P_{i-1} + \angle P_i + \angle P_{i+1} + \dots \quad (19)$$

where $\angle P_{i-1}, \angle P_i, \angle P_{i+1}, \dots$ are the adjacent field angles with the same value of light transmission.

Consider that the LTM defined in (18) is only suitable for the situation of partial transparency, as shown in Fig. 3, which probably leads UAV $\alpha_{ij}^{B_{lk}}$ to a wrong path called dead-end channel (arrive at point P). Here, partial transparency can be understood as the UAV can detect the feasible routes with certain light transmission when the obstacles are in front of it. And the flyable space of the UAV decreases as the distance between the UAV and obstacle decreases. When the flyable space of the UAV approaches zero, it can be considered that the UAV has entered the dead-end channel. Therefore, a distance factor must be added to (18) to help the UAVs avoid falling into the dead-end channel, which can be defined as

$$\lambda = \begin{cases} e^{\delta_M \cdot \| \mathbf{q}_{ij}^{\alpha B_{lk}} - \mathbf{q}_\nu^o \|}, & \text{if } \alpha_{ij}^{B_{lk}} \notin B \\ e^{\delta_B \cdot \| \mathbf{q}_{ij}^{\alpha B_{lk}} - \mathbf{q}_\nu^o \|}, & \text{if } \alpha_{ij}^{B_{lk}} \in B \end{cases} \quad (20)$$

where δ_M and δ_B are the weight coefficients of distance factor ($\delta_M > 0, \delta_B > 0$) for the UAV located in the swarm middle and boundary, respectively. The larger the values of δ_M and δ_B are, the greater influence of the distance factor on the LTM is,

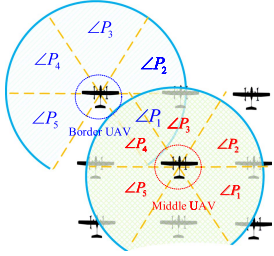


Fig. 4. Middle UAV and border UAV (Left).

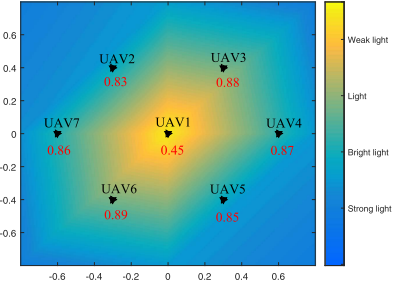


Fig. 5. Light transmission in a UAV formation (Right).

and vice versa; B is a set of UAVs located at the boundary of formation.

In a largely dense swarm, it is defined that the UAV in the middle is surrounded by its neighbors, whose all-view field will be occlusive. On the contrary, when the UAV is located at the boundary, there is at least one interval of the five field angles as the maneuverable space. In this way, the UAV can judge its position in the swarm. The characteristics of the UAVs located at the middle and boundary of the swarm are shown in Fig. 4. In this way, we can get the final LTM expression as

$$P(\alpha_{ij}^{B_{lk}}) = \frac{3A(\alpha_{ij}^{B_{lk}})}{5\pi} \cdot \lambda \\ = \begin{cases} \frac{3A(\alpha_{ij}^{B_{lk}})}{5\pi} \cdot e^{\delta_M \cdot \|q_{ij}^{\alpha B_{lk}} - q_\nu^o\|}, & \text{if } \alpha_{ij}^{B_{lk}} \notin B \\ \frac{3A(\alpha_{ij}^{B_{lk}})}{5\pi} \cdot e^{\delta_B \cdot \|q_{ij}^{\alpha B_{lk}} - q_\nu^o\|}, & \text{if } \alpha_{ij}^{B_{lk}} \in B \end{cases} \quad (21)$$

Fig. 5 shows the numerical values of light transmission in a UAV formation, which are indicated by the red text.

III. IMPROVED POTENTIAL FIELD FUNCTIONS DESIGN

In this section, the improved potential field functions are designed based on the interaction between UAVs, obstacle collision avoidance, and swarm structure maintenance, respectively. To overcome the inherent shortcomings of potential field function with nonreachable and local minima, the LTM is introduced to improve the functions, which can achieve a better control effect in the swarm control.

To begin, considering that the Euclidean norm is not differentiable at zero, the σ -norm is adopted to construct a nonnegative smooth potential function between two UAVs [34]. The σ -norm is defined as

$$\|z\|_\sigma = \frac{1}{\epsilon} \left[\sqrt{1 + \epsilon \|z\|^2} - 1 \right] \quad (22)$$

where the σ -norm of a vector is a map of $\mathbb{R}^n \rightarrow \mathbb{R}^+$; parameters $\epsilon > 0$. And a gradient $\sigma_\epsilon(z)$ can be expressed as

$$\sigma_\epsilon(z) = \nabla \|z\|_\sigma = \frac{z}{\sqrt{1 + \epsilon \|z\|^2}}. \quad (23)$$

A. Interaction Between UAVs

The derivable potential field function between UAVs can be defined as

$$\psi^\alpha \left(\left\| q_{ij,pq}^{\alpha\alpha B_{lk}} \right\|_\sigma \right) = C_1 \int_{\|d\|_\sigma}^{\left\| q_{ij,pq}^{\alpha\alpha B_{lk}} \right\|_\sigma} \rho_\eta^\alpha \left(\frac{s}{\|r_\alpha\|_\sigma} \right) w_1(s) ds \quad (24)$$

where

$$q_{ij,pq}^{\alpha\alpha B_{lk}} = q_{ij}^{\alpha B_{lk}} - q_{pq}^{\alpha B_{lk}} \quad (ij \neq pq) \quad (25)$$

and $\|d\|_\sigma$ is the desired distance between two UAVs. The value of potential field function will tend to the globally unique minimum when the two UAVs maintain the desired distance $\|d\|_\sigma$. The term C_1 can be expressed as

$$C_1 = 1 + \tau_1 P(\alpha_{ij}^{B_{lk}}) \quad (26)$$

where τ_1 is the correlation coefficient of LTM; and $P(\alpha_{ij}^{B_{lk}})$ is the LTM. The term $w_1(s)$ can be denoted as

$$w_1(s) = \frac{s - \|d\|_\sigma}{\sqrt{1 - (s - \|d\|_\sigma)^2}}. \quad (27)$$

The collision function $\rho_\eta^\alpha(s)$ between UAVs can be written as

$$\rho_\eta^\alpha(s) = \begin{cases} 1, & s \in [0, \eta) \\ \frac{1}{2} \left[1 + \cos(\pi \frac{s-\eta}{1-\eta}) \right], & s \in [\eta, 1] \\ 0, & \text{otherwise} \end{cases} \quad (28)$$

where $\eta \in (0, 1)$.

The potential field function designed in (24) satisfies the following conditions.

- 1) When $\|q_{ij,pq}^{\alpha\alpha B_{lk}}\|_\sigma \geq \|r_\alpha\|_\sigma$, this potential field function remains a constant.
- 2) When $\|q_{ij,pq}^{\alpha\alpha B_{lk}}\|_\sigma < \|d\|_\sigma$, UAV $\alpha_{ij}^{B_{lk}}$ excludes UAV $\alpha_{pq}^{B_{lk}}$ in the same group.
- 3) When $\|d\|_\sigma < \|q_{ij,pq}^{\alpha\alpha B_{lk}}\|_\sigma < \|r_\alpha\|_\sigma$, UAV $\alpha_{ij}^{B_{lk}}$ attracts UAV $\alpha_{pq}^{B_{lk}}$.

B. Obstacle Collision Avoidance

The derivable potential field function between a UAV and an obstacle can be defined as

$$\psi^o \left(\left\| q_{ij,\nu}^{\alpha o B_{lk}} \right\|_\sigma \right) = C_2 \int_{\|r_o\|_\sigma}^{\left\| q_{ij,\nu}^{\alpha o B_{lk}} \right\|_\sigma} \rho_\eta^o \left(\frac{s}{\|r_o\|_\sigma} \right) w_2(s) ds \quad (29)$$

where

$$q_{ij,\nu}^{\alpha o B_{lk}} = q_{ij}^{\alpha B_{lk}} - q_\nu^o. \quad (30)$$

The value of this potential field function will tend to 0 when the obstacle is outside the repulsion radius $\|r_o\|_\sigma$. The term C_2 can be expressed as

$$C_2 = 1 + \frac{\tau_2}{P(\alpha_{ij}^{B_{lk}})} \quad (31)$$

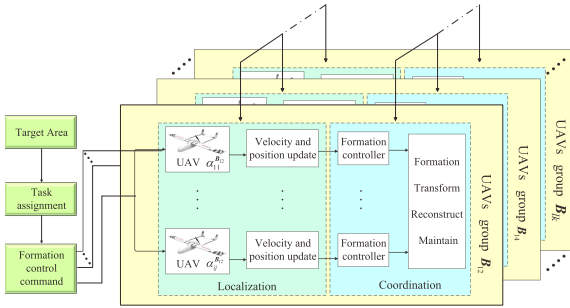


Fig. 6. Diagram for control system.

where τ_2 is the correlation coefficient of LTM. The term $w_2(s)$ can be denoted as

$$w_2(s) = \frac{s - \|r_o\|_\sigma}{s^3}. \quad (32)$$

The collision function of the obstacle to the UAV can be written as

$$\rho^o(s) = \begin{cases} 1 & , s \in [0, 1] \\ 0 & , \text{otherwise} \end{cases}. \quad (33)$$

When $\|\mathbf{q}_{ij,\nu}^{\alpha o B_{lk}}\|_\sigma \rightarrow 0$, this potential field function tends to ∞ , where $\|\mathbf{q}_{ij,\nu}^{\alpha o B_{lk}}\|_\sigma \in (0, \|r_o\|_\sigma]$. That is to say, UAV $\alpha_{ij}^{B_{lk}}$ stays away from the obstacle under the action of repulsive force when it approaches obstacles.

C. Swarm Structure Maintenance

The derivable potential field function between a UAV and a reference point of swarm structure can be defined as

$$\psi^r \left(\left\| \hat{\mathbf{q}}_{ij}^{\alpha B_{lk}} \right\|_\sigma \right) = \int_0^{\left\| \hat{\mathbf{q}}_{ij}^{\alpha B_{lk}} \right\|_\sigma} s ds \quad (34)$$

where

$$\hat{\mathbf{q}}_{ij}^{\alpha B_{lk}} = \mathbf{q}_{ij}^{\alpha B_{lk}} - \mathbf{q}^r - \xi_{ij}^{\alpha B_{lk}} \Delta \mathbf{q}_{ij}^{\alpha B_{lk}}. \quad (35)$$

When $\|\mathbf{q}_{ij}^{\alpha B_{lk}} - \mathbf{q}^r - \xi_{ij}^{\alpha B_{lk}} \Delta \mathbf{q}_{ij}^{\alpha B_{lk}}\|_\sigma \rightarrow 0$, this potential field function tends to 0.

IV. SWARM ALGORITHMS

A. Preparation

As mentioned above, architecture of group control is proposed in this article. Fig. 6 shows the control structure of the swarm. For a clearer presentation, combining (25), (30), and (35), we can define the following:

$$\begin{cases} \hat{\mathbf{q}}_{ij,pq}^{\alpha o B_{lk}} = \mathbf{q}_{ij,pq}^{\alpha o B_{lk}} & (i = 1, \dots, n_l; j = 1, \dots, m_k) \\ \hat{\mathbf{q}}_{ij,\nu}^{\alpha o B_{lk}} = \mathbf{q}_{ij,\nu}^{\alpha o B_{lk}} \end{cases} \quad (36)$$

It follows that the second-order integral system model of UAV $\alpha_{ij}^{B_{lk}}$ in (11) can be rewritten as

$$\begin{cases} \dot{\hat{\mathbf{q}}}_{ij}^{\alpha B_{lk}} = \hat{\mathbf{p}}_{ij}^{\alpha B_{lk}} \\ \dot{\hat{\mathbf{p}}}_{ij}^{\alpha B_{lk}} = \hat{\mathbf{u}}_{ij}^{\alpha B_{lk}} \end{cases} \quad (i = 1, \dots, n_l; j = 1, \dots, m_k) \quad (37)$$

where

$$\hat{\mathbf{p}}_{ij}^{\alpha B_{lk}} = \mathbf{p}_{ij}^{\alpha B_{lk}} - \mathbf{p}^r. \quad (38)$$

Lemma 1: [38] $G = (v, \varepsilon)$ is an undirected graph of order n with a nonnegative adjacency matrix $A = A^T$. Then, L is a

positive semidefinite matrix that satisfies the following sum-of-squares (SOS) property:

$$(\hat{\mathbf{p}}^\alpha)^T (L(t) \otimes I_n) (\hat{\mathbf{p}}^\alpha) = \frac{1}{2} \sum_{\Gamma} a_{ij,pq}(t) (\hat{\mathbf{p}}_{ij,pq}^{\alpha o B_{lk}})^T \hat{\mathbf{p}}_{ij,pq}^{\alpha o B_{lk}} \quad (39)$$

where $\Gamma = \{(\alpha_{ij}^{B_{lk}}, \alpha_{pq}^{B_{lk}}) \in \varepsilon(t)\}$.

Lemma 2: [39] (LaSalle's principle) Let $L: \mathbb{R}^n \rightarrow \mathbb{R}$ be a locally positive definite function such that on the compact set, $\Omega_c = \{x \in \mathbb{R}^n : L(x) \leq C\}$ (C is a constant greater than 0). If $\dot{L}(x) \leq 0$ is satisfied, then

$$S = \{x \in \Omega_c : \dot{L}(x) = 0\}. \quad (40)$$

As $t \rightarrow \infty$, the trajectory tends to the largest invariant set inside S . In particular, if S contains no invariant sets other than $x = 0$, then 0 is an only equilibrium point.

B. Control Algorithm of Swarm

To achieve collaborative autonomy in the swarm, the swarm control algorithm for each UAV is designed, in which the swarm structure maintenance and speed consistency control are considered.

$$\begin{aligned} \hat{\mathbf{u}}_{ij}^{\alpha B_{lk}} = & - \sum_{N_{pq}^{\alpha B_{lk}}(t)} \nabla \left(\hat{\mathbf{q}}_{ij,pq}^{\alpha o B_{lk}} \right) \psi^\alpha \left(\left\| \hat{\mathbf{q}}_{ij,pq}^{\alpha o B_{lk}} \right\|_\sigma \right) \\ & + \sum_{N_{pq}^{\alpha B_{lk}}(t)} a_{ij,pq}(t) \hat{\mathbf{p}}_{ij,pq}^{\alpha o B_{lk}} \\ & - \sum_{N_{ij}^o(t)} \nabla \left(\hat{\mathbf{q}}_{ij,\nu}^{\alpha o B_{lk}} \right) \psi^o \left(\left\| \hat{\mathbf{q}}_{ij,\nu}^{\alpha o B_{lk}} \right\|_\sigma \right) \\ & - \nabla \left(\hat{\mathbf{q}}_{ij}^{\alpha B_{lk}} \right) \psi^r \left(\left\| \hat{\mathbf{q}}_{ij}^{\alpha B_{lk}} \right\|_\sigma \right) - c_4 \hat{\mathbf{p}}_{ij}^{\alpha B_{lk}}. \end{aligned} \quad (41)$$

C. Stability Analysis of Swarm

Theorem 1: Consider a UAV swarm consisting of $a \times b$ groups, such as B_{lk} in (4), including $n_l \times m_k$ UAVs whose model can be described as (37). Then, under the swarm control algorithm in (41), the following statements hold.

- 1) (*Convergence*) The energy of the swarm system is non-increasing, which means the control algorithm proposed in (41) is convergent. And the total energy of the swarm system cannot exceed the initial energy L_0 ($L_0 = C$).
- 2) (*Consistency*) The speeds of the UAVs in each group tend to the same value p^r when the swarm system tends to be stable.
- 3) (*No collision*) There is no collision between any two UAVs, and between any UAV and any obstacle.

The proof of Theorem 1 is given in Appendix C.

V. SIMULATION

In this section, we provide simulation results to illustrate the effectiveness of the proposed control algorithm and compare it with the conventional control method of collision avoidance designed in the existing literature.

A. Preliminaries of Simulation

Consider a UAV swarm consisting of 360 fixed wing UAVs, which was divided into 40 groups. The structure of this UAV

swarm is described as matrix $\Xi_{n \times m}$ in (2), where the partitioned matrices B_{lk} consists of nine UAVs.

1) *Communication Graph*: For the UAVs in partitioned matrices B_{lk} , the following communication topology was designed, whose Laplacian matrix is:

$$L = \begin{bmatrix} 3 & -1 & 0 & -1 & -1 & 0 & 0 & 0 & 0 \\ -1 & 4 & -1 & 0 & -1 & -1 & 0 & 0 & 0 \\ 0 & -1 & 2 & 0 & 0 & -1 & 0 & 0 & 0 \\ -1 & 0 & 0 & 4 & -1 & 0 & -1 & -1 & 0 \\ -1 & -1 & 0 & -1 & 6 & -1 & 0 & -1 & -1 \\ 0 & -1 & -1 & 0 & -1 & 4 & 0 & 0 & -1 \\ 0 & 0 & 0 & -1 & 0 & 0 & 2 & -1 & 0 \\ 0 & 0 & 0 & -1 & -1 & 0 & -1 & 4 & -1 \\ 0 & 0 & 0 & 0 & -1 & -1 & 0 & -1 & 3 \end{bmatrix}. \quad (42)$$

2) *Parameters*: For the initial configuration, we set the spacing interval between UAVs in one group to 1.5 m, which is because of the movement restriction about the minimum turning radius of each UAV, namely $dx = dy = 1.5$ m. It is desired that the UAV swarm ultimately achieves the fly task from area A to area B of the x - y plane while keeping the swarm structure without collision during the flight process, where the areas are

$$A: = \{(x_1, y_1) \in A | 0 \leq x_1 \leq 50, -30 \leq y_1 \leq 20\} \quad (43)$$

$$B: = \{(x_2, y_2) \in B | 90 \leq x_2 \leq 140, 90 \leq y_2 \leq 140\}. \quad (44)$$

The initial positions of the UAVs were randomly generated within a certain position interval. And the flight constraints of the fixed-wing UAV were designed as follows: the minimum speed $v_{\min}^{\alpha B_{lk}}$ and maximum speed $v_{\max}^{\alpha B_{lk}}$ of UAV $\alpha_i^{\alpha B_{lk}}$ are 0.2 m/s and 1 m/s, respectively; the minimum turning radius is 0.5 m; and the maximum overload is 10 G. For the weight coefficients of LTM distance factor in (21), we set $\delta_C = 0.4$ and $\delta_B = 0.8$; the correlation coefficient of LTM $c_0 = 0.4$, $c_1 = 0.25$. And some distance settings in the simulation are $\|r_\alpha\|_\sigma = 10$ m and $\|r_o\|_\sigma = 1.2$ m, respectively.

B. Simulation Result Analysis

1) *Verification Simulation*: In this section, several numerical simulations were conducted to illustrate the rationality of theoretical results and the validity of the control algorithm in UAV swarm.

a) *Formation action without obstacles*: At first, the stability and consistency of the flight process for the UAV swarm without the influence of obstacles were verified. Here, the same color is used to represent a group of curve changes.

Fig. 7(a) is the speed curves of all UAVs in the swarm, which shows the speed of 360 UAVs can eventually converge to the p^r ($p^r = 0.4$ m/s) and the maximum speed do not exceed 1 m/s. That is, the swarm system has good performance in speed consistency with the proposed control algorithm.

Fig. 7(b) shows the position errors between all UAVs and the reference point of the swarm structure, which show that the errors will eventually converge to 0. That is, the swarm can eventually converge to the desired structure, whereas the UAVs can keep the desired distance during the flight. These results confirm the convergence of the speeds of the UAV in the swarm. When $t \rightarrow \infty$, the energies J_{ψ^α} , J_{ψ^o} , and J_{ψ^r} are the lowest. In the meanwhile, the swarm system can keep the energy at the lowest state.

The flight path of the UAV swarm is shown in Fig. 7(c), where each triangle represents a UAV and the circle is the range within which a single UAV can safely fly. The flight trajectories of

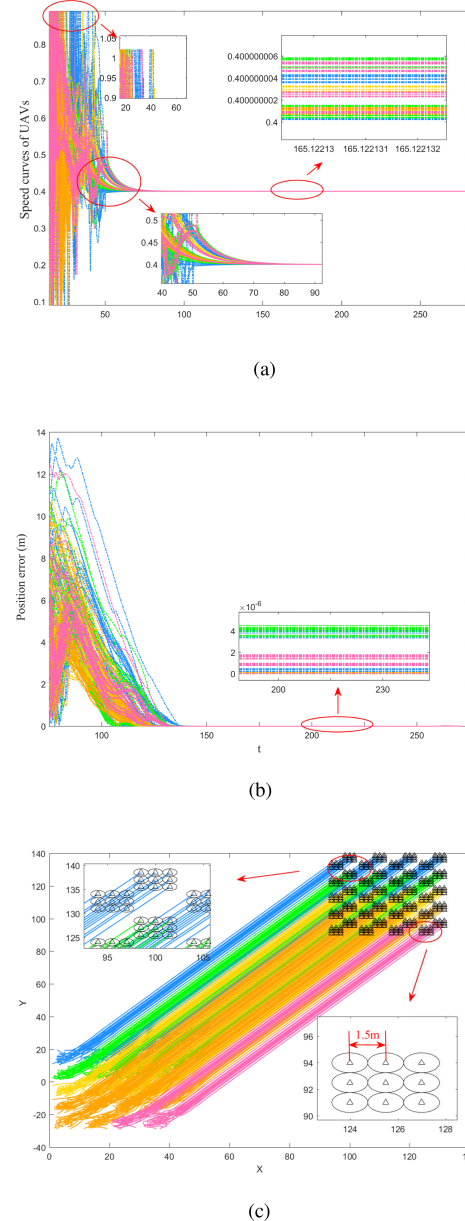


Fig. 7. Simulation results of the UAV swarm without obstacles. (a) Speed curves of UAVs. (b) Position error. (c) Flight path.

different UAV groups were recorded by colored lines. The results show that the swarm can reach the destination in the desired structure without UAV collision. In this way, the statement of no collision in Theorem 1 has been proved.

b) *Formation action with several obstacles*: In this part, the obstacle avoidance performance of the UAV swarm was verified by setting some random obstacles, which are also used to verify the reconstruction and maintenance performance of the swarm structure.

Fig. 8 is the flight path of the UAV swarm under the obstacle environment. In the figure, the positions of the obstacles were represented by solid circles, and the UAVs were still represented by a triangle. The results show that the UAV swarm can bypass the obstacles under the action of the LTM and the force of obstacle repulsion; in the meanwhile, there is no collision in the UAV swarm. In addition, only a part of the swarm rather than the whole is affected by obstacles when meeting

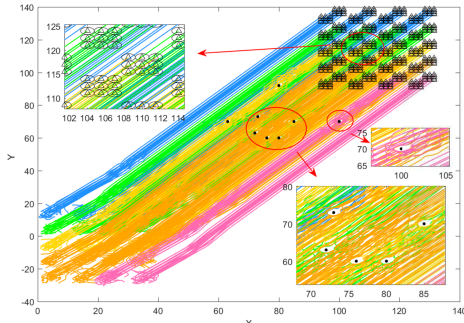


Fig. 8. Flight path of the UAV swarm with obstacles.

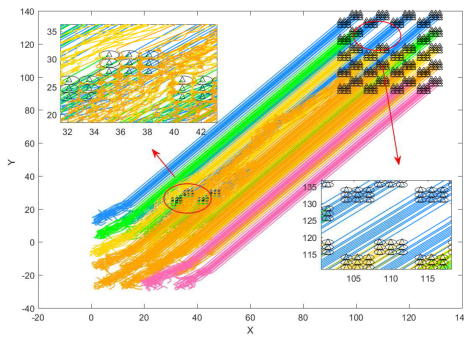


Fig. 9. Flight path of the UAV swarm with some breakdown.

the obstacles, where we have reserved the maneuver space for avoiding the collision in advance. The maximum, minimum, and average position errors of the swarm avoidance obstacle process are about 17.3, 0, and 1.2 m, respectively. In other words, the designed models and swarm control algorithms have a better ability to cope with the collision and avoidance of UAV swarm, especially in large scale.

During the movement, it can be found that the UAVs fly in the direction of strong light under the action of the APF method based on LTM. At the same time, UAVs do not collide with adjacent UAVs via accessing the reserved maneuvering space for adjustment. Therefore, the validity of the proposed desired formation is proved. Besides, it can be seen from the flight path of the swarm in Fig. 8 that the statement of Theorem 1 still holds in the presence of obstacles.

c) *Broken down of several UAVs:* To further test the reliable ability of obstacle avoidance and reconstruction capabilities of the swarm, the case that several UAV groups are broken down in the flight process was set.

Suppose that four UAV groups in the middle of the swarm are broken down and cannot receive the swarm commands normally at $t = 150$, which leads to the groups being detained in the air and go straight east with the minimum speed. In this case, the failed groups will be considered as obstacles for other UAVs.

Fig. 9 is the flight path of the UAV swarm with some breakdown, which shows that UAVs without malfunction can bypass the failed UAVs and reach the target area smoothly with the desired formation. The partial moving processes of serval breakdown UAVs are shown in Fig. 10. Here, blue markers were used to refer to the destroyed UAVs.

It can be seen from the simulation under this situation that the architecture based on grouping control has better fault tolerance. Even if some individual groups fail, they will not affect the flight

of the entire swarm. In this way, the flight cost of the swarm is the least and the energy consumption is also minimal.

Therefore, there has a well confirmation of the theoretical and simulation results based on the situation mentioned in Sections V-B1.a)–c), which means the swarm system has good consistency and coordination in formation maneuver and collision avoidance.

2) *Simulation for Comparison:* To verify the superiority of the proposed collision avoidance control method, we compared the flight performance of the UAV swarm under the conventional potential field function and the proposed control architecture in this article.

Fig. 11 is the result for the conventional method, where the potential field function method in [34] is the most commonly used method in UAV swarm obstacle avoidance. Besides, this method is also the most similar control algorithm to that in this article, whereas other methods, such as model predictive control, speed barrier method, and Markov decision method, are all not suitable for large-scale swarm control, which have been introduced in the introduction. Here, the obstacle settings, simulation initial conditions, and parameters are the same as mentioned in Section V-B1.b.

To analyze and compare the experimental results more intuitively, we defined the following indicators to measure the results.

- 1) Swarm convergence time after passing the obstacle avoidance area to target area T_o : The shorter the convergence time of the swarm is, the faster the system can reach the lowest energy point. At this time, the swarm can fly stably in the desired formation.
- 2) The number of UAVs with the same final speed N_u : When the speeds of all UAVs in the swarm are the same, the consistency is reached.
- 3) Obstacle avoidance success rate γ : We define $\gamma = \frac{N_s}{N_t}$, where, N_s is the number of UAVs surviving after obstacle avoidance; N_t is the UAVs number in the swarm. The larger the γ is, the better the obstacle avoidance performance of the algorithm is.
- 4) Program running time T_p : Under the same simulation platform, the shorter the program running time is, the lower the computational complexity is. So the program is more suitable for large-scale systems. Here, the simulation platform is equipped with Intel Core i5-9300H-class CPU, 16 G memory, and 512 G solid-state hard disk.
- 5) The average flight path length of the UAV P_u : When the flight distance is shorter, the trajectory is smoother and the trajectory cost is smaller.
- 6) Maximum radius of curvature in swarm flight k_u : When the radius of curvature is larger, the ability of the UAV's overload also needs to be improved accordingly. In this way, the smaller the radius of curvature, the more stable the system can be.

It can be seen from Fig. 11 that the flight path of the UAV swarm is bumpy, the trajectory cost is high, and the desired structure cannot be formed completely. During the obstacle avoidance process, the UAVs are bouncing away from the obstacle instead of smoothly avoiding obstacles. That is, the conventional method has extremely high requirements for UAVs overload, which is even not suitable for fixed-wing UAV obstacle avoidance. From the performance comparison in Table I, we can conclude that the proposed method has bigger performance improvement compared to the existing method.

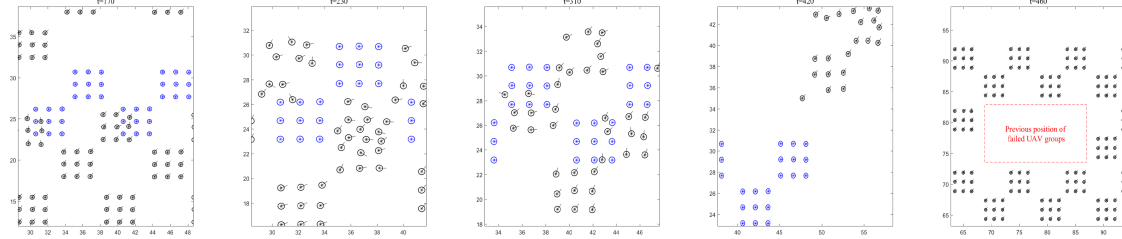


Fig. 10. Partial moving process of several UAVs breakdown.

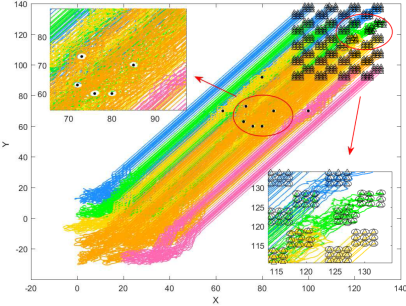


Fig. 11. Flight path of UAV swarm with conventional method.

TABLE I
COMPARISON OF SIMULATION RESULTS

Indicator	This paper	Method in [34]	Improvement
T_o (s)	4.5	NaN ¹	95%
N_u	360	337	6.8%
γ	100%	97%	3.0%
T_p (s)	15.3	23.5	53.6%
P_u (Km)	152	164	7.9%
k_u (Km $^{-1}$)	12	34	88.9%

1. NaN refers to the formation system was not fully converged in the end.

VI. CONCLUSION

In this article, a collision avoidance and formation control algorithm for a large-scale fixed-wing UAV swarm based on the reserved maneuvering space has been designed, which can guarantee the safety and survivability of UAVs via effectively avoiding obstacles while maintaining the stability of the swarm. Under the distributed control architecture, a new swarm structure has been proposed, which cooperates with the LTM to find a feasible flying route for UAVs in time. Furthermore, the improved potential field functions and the swarm control algorithms for UAVs have been designed. Finally, the simulation results show that the control algorithms have good advantages in collision, obstacle avoidance, system stability maintenance, and rapid formation reconstruction, and also have a better performance than the methods in the existing literature. In future research, we will proceed from the actual flight verification and the rapid turn of the swarm based on such structure, respectively.

APPENDIX A ALGORITHM FLOW

Algorithm 1: The Algorithm Flow of the Swarm System.

Input: Target area, Desired swarm formation, Obstacle location.

Output: The result of swarm flight.

- Step 1:** Divide the swarm into several groups;
- Step 2:** Form initial Desired swarm formation and move in the Target area direction;
- Step 3:** Swarm member current state update and get their location in swarm formation dynamically;
- Step 4:** Swarm member coordinate the velocity and location with other UAV;
- Step 5:** Swarm avoid obstacles in real time during flight; **if** Distance between UAVs and obstacles is less than the safety distance **then**
 - UAVs find maneuverable space and avoid obstacles based on APF, improving via LTM;**else**
 - if** Arrive at the destination **then**
 - Complete the task
 - else**
 - Back to Step 3.
 - end if****end if**
- Step 6:** Record the fly path of swarm formation.

APPENDIX B CONSTRUCTION OF UAV MODEL

Suppose that the simplified dynamic model of UAV $\alpha_{ij}^{B_{lk}}$ can be expressed as

$$\begin{cases} \dot{x}_{ij}^{\alpha B_{lk}} = v_{ij}^{\alpha B_{lk}} \cos \varphi_{ij}^{\alpha B_{lk}} \\ \dot{y}_{ij}^{\alpha B_{lk}} = v_{ij}^{\alpha B_{lk}} \sin \varphi_{ij}^{\alpha B_{lk}} \\ \dot{v}_{ij}^{\alpha B_{lk}} = n_{ij}^{v\alpha B_{lk}} \\ \dot{\psi}_{ij}^{\alpha B_{lk}} = n_{ij}^{\psi\alpha B_{lk}} \end{cases} \quad (45)$$

where $(x_{ij}^{\alpha B_{lk}}, y_{ij}^{\alpha B_{lk}})$ is the position of UAV $\alpha_{ij}^{B_{lk}}$ in the inertial coordinate system; $\varphi_{ij}^{\alpha B_{lk}}$ is the heading angle of UAV $\alpha_{ij}^{B_{lk}}$; $n_{ij}^{v\alpha B_{lk}}$ and $n_{ij}^{\psi\alpha B_{lk}}$ are the control inputs that represent the overload of the UAV $\alpha_{ij}^{B_{lk}}$ in the inertial coordinate system; and $v_{ij}^{\alpha B_{lk}}$ is the velocity of UAV $\alpha_{ij}^{B_{lk}}$. The schematic diagram of fixed-wing UAV flight is shown in Fig. 12.

To simplify the UAV model, we need to linearize (45). As mentioned above $q_{ij}^{\alpha B_{lk}} = [x_{ij}^{\alpha B_{lk}} \quad y_{ij}^{\alpha B_{lk}}]^T$, and calculating its first time derivative, we have

$$\dot{p}_{ij}^{\alpha B_{lk}} = \dot{q}_{ij}^{\alpha B_{lk}} = \begin{bmatrix} \dot{x}_{ij}^{\alpha B_{lk}} \\ \dot{y}_{ij}^{\alpha B_{lk}} \end{bmatrix} = \begin{bmatrix} v_{ij}^{\alpha B_{lk}} \cos \varphi_{ij}^{\alpha B_{lk}} \\ v_{ij}^{\alpha B_{lk}} \sin \varphi_{ij}^{\alpha B_{lk}} \end{bmatrix}. \quad (46)$$

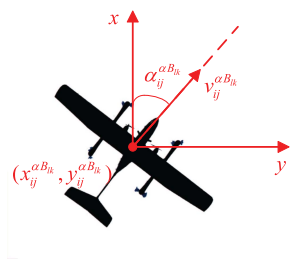


Fig. 12. Schematic diagram of a fixed-wing UAV flight.

Further, calculating the first derivative of formula (46), we have

$$\begin{aligned} \dot{p}_{ij}^{\alpha B_{lk}} &= \ddot{q}_{ij}^{\alpha B_{lk}} = \begin{bmatrix} \ddot{x}_{ij}^{\alpha B_{lk}} \\ \ddot{y}_{ij}^{\alpha B_{lk}} \end{bmatrix} \\ &= \begin{bmatrix} \dot{v}_{ij}^{\alpha B_{lk}} \cos \varphi_{ij}^{\alpha B_{lk}} - v_{ij}^{\alpha B_{lk}} \dot{\varphi}_{ij}^{\alpha B_{lk}} \sin \varphi_{ij}^{\alpha B_{lk}} \\ \dot{v}_{ij}^{\alpha B_{lk}} \sin \varphi_{ij}^{\alpha B_{lk}} + v_{ij}^{\alpha B_{lk}} \dot{\varphi}_{ij}^{\alpha B_{lk}} \cos \varphi_{ij}^{\alpha B_{lk}} \end{bmatrix} \\ &= \begin{bmatrix} \cos \varphi_{ij}^{\alpha B_{lk}} & -v_{ij}^{\alpha B_{lk}} \sin \varphi_{ij}^{\alpha B_{lk}} \\ \sin \varphi_{ij}^{\alpha B_{lk}} & v_{ij}^{\alpha B_{lk}} \cos \varphi_{ij}^{\alpha B_{lk}} \end{bmatrix} \begin{bmatrix} n_{ij}^{v\alpha B_{lk}} \\ n_{ij}^{\varphi\alpha B_{lk}} \end{bmatrix}. \end{aligned} \quad (47)$$

Then, define

$$\begin{aligned} H_{ij}^{\alpha B_{lk}} &= \begin{bmatrix} \cos \varphi_{ij}^{\alpha B_{lk}} & -v_{ij}^{\alpha B_{lk}} \sin \varphi_{ij}^{\alpha B_{lk}} \\ \sin \varphi_{ij}^{\alpha B_{lk}} & v_{ij}^{\alpha B_{lk}} \cos \varphi_{ij}^{\alpha B_{lk}} \end{bmatrix} \\ n_{ij}^{\alpha B_{lk}} &= \begin{bmatrix} n_{ij}^{v\alpha B_{lk}} & n_{ij}^{\varphi\alpha B_{lk}} \end{bmatrix}^T \\ u_{ij}^{\alpha B_{lk}} &= \begin{bmatrix} u_{ij}^{v\alpha B_{lk}} & u_{ij}^{\varphi\alpha B_{lk}} \end{bmatrix}^T. \end{aligned} \quad (48)$$

It follows that

$$u_{ij}^{\alpha B_{lk}} = H_{ij}^{\alpha B_{lk}} n_{ij}^{\alpha B_{lk}}. \quad (49)$$

Therefore, the relationship between the original control input $n_{ij}^{\alpha B_{lk}}$ and the new input $u_{ij}^{\alpha B_{lk}}$ is as follows:

$$n_{ij}^{\alpha B_{lk}} = H_{ij}^{\alpha B_{lk}}^{-1} u_{ij}^{\alpha B_{lk}}. \quad (50)$$

Therefore, (46) and (47) can be transformed into the second-order integral system in (11).

APPENDIX C PROOF OF THEOREM 1

A. Proof of Convergence

The energy function of the swarm system can be defined as

$$\begin{aligned} L &= \sum_{l=1}^a \sum_{k=1}^b \left\{ \sum_{i=1}^{n_l} \sum_{j=1}^{m_k} \left[\sum_{p=1}^{n_l} \sum_{q=1}^{m_k} \frac{1}{2C_1} \psi^\alpha \left(\left\| \hat{q}_{ij,pq}^{\alpha\alpha B_{lk}} \right\|_\sigma \right) \right. \right. \\ &\quad \left. \left. + \sum_{t=1}^{N_o} \frac{1}{C_2} \psi^o \left(\left\| \hat{q}_{ij,\nu}^{\alpha o B_{lk}} \right\|_\sigma \right) \right] + \sum_{i=1}^{n_l} \sum_{j=1}^{m_k} \left[\psi^r \left(\left\| \hat{q}_{ij}^{\alpha B_{lk}} \right\|_\sigma \right) \right. \right. \\ &\quad \left. \left. + \frac{1}{2} \left(\hat{p}_{ij}^{\alpha B_{lk}} \right)^T \hat{p}_{ij}^{\alpha B_{lk}} \right] \right\}. \end{aligned} \quad (51)$$

According to the symmetry of the potential field function ψ^α designed in (24) between the two UAVs, we can get

$$\begin{aligned} \frac{\partial \psi^\alpha \left(\left\| \hat{q}_{ij,pq}^{\alpha\alpha B_{lk}} \right\|_\sigma \right)}{\partial \left(\hat{q}_{ij,pq}^{\alpha\alpha B_{lk}} \right)} &= \frac{\partial \psi^\alpha \left(\left\| \hat{q}_{ij,pq}^{\alpha\alpha B_{lk}} \right\|_\sigma \right)}{\partial \left(\hat{q}_{ij}^{\alpha B_{lk}} \right)} \\ &= -\frac{\partial \psi^\alpha \left(\left\| \hat{q}_{ij,pq}^{\alpha\alpha B_{lk}} \right\|_\sigma \right)}{\partial \left(\hat{q}_{pq}^{\alpha B_{lk}} \right)}. \end{aligned} \quad (52)$$

It follows from (52) that the time derivative of the potential field function ψ^α can be calculated as

$$\begin{aligned} \frac{d\psi^\alpha \left(\left\| \hat{q}_{ij,pq}^{\alpha\alpha B_{lk}} \right\|_\sigma \right)}{dt} &= 2C_1 \left(\hat{p}_{ij}^{\alpha B_{lk}} \right)^T \nabla \left(\hat{q}_{ij,pq}^{\alpha\alpha B_{lk}} \right) \\ &\quad \cdot \psi^\alpha \left(\left\| \hat{q}_{ij,pq}^{\alpha\alpha B_{lk}} \right\|_\sigma \right). \end{aligned} \quad (53)$$

Similarly, the time derivative of the potential field function ψ^o in (29) and ψ^r in (34) can be calculated as

$$\begin{aligned} \frac{d\psi^o \left(\left\| \hat{q}_{ij,t}^{\alpha o B_{lk}} \right\|_\sigma \right)}{dt} &= C_2 \left(\hat{p}_{ij}^{\alpha B_{lk}} \right)^T \nabla \left(\hat{q}_{ij,\nu}^{\alpha o B_{lk}} \right) \\ &\quad \cdot \psi^o \left(\left\| \hat{q}_{ij,\nu}^{\alpha o B_{lk}} \right\|_\sigma \right) \end{aligned} \quad (54)$$

$$\frac{d\psi^r \left(\left\| \hat{q}_{ij}^{\alpha B_{lk}} \right\|_\sigma \right)}{dt} = \left(\hat{p}_{ij}^{\alpha B_{lk}} \right)^T \nabla \left(\hat{q}_{ij}^{\alpha B_{lk}} \right) \psi^r \left(\left\| \hat{q}_{ij}^{\alpha B_{lk}} \right\|_\sigma \right). \quad (55)$$

If we plug (53)–(55) back into the first-order time derivative of (51), the time derivative of the swarm energy function can be obtained as follows:

$$\begin{aligned} \dot{L} &= \sum_{l=1}^a \sum_{k=1}^b \left\{ \sum_{i=1}^{n_l} \sum_{j=1}^{m_k} \sum_{p=1}^{n_l} \sum_{q=1}^{m_k} \left(\hat{p}_{ij}^{\alpha B_{lk}} \right)^T \right. \\ &\quad \cdot \nabla \left(\hat{q}_{ij,pq}^{\alpha\alpha B_{lk}} \right) \psi^\alpha \left(\left\| \hat{q}_{ij,pq}^{\alpha\alpha B_{lk}} \right\|_\sigma \right) \\ &\quad + \sum_{i=1}^{n_l} \sum_{j=1}^{m_k} \sum_{p=1}^{n_l} \sum_{q=1}^{m_k} \cdot \left(\hat{p}_{ij}^{\alpha B_{lk}} \right)^T \nabla \left(\hat{q}_{ij,\nu}^{\alpha o B_{lk}} \right) \\ &\quad \psi^o \left(\left\| \hat{q}_{ij,\nu}^{\alpha o B_{lk}} \right\|_\sigma \right) \\ &\quad + \sum_{i=1}^{n_l} \sum_{j=1}^{m_k} \left[\left(\hat{p}_{ij}^{\alpha B_{lk}} \right)^T \nabla \left(\hat{q}_{ij}^{\alpha B_{lk}} \right) \cdot \psi^r \left(\left\| \hat{q}_{ij}^{\alpha B_{lk}} \right\|_\sigma \right) \right. \\ &\quad \left. + \left(\hat{p}_{ij}^{\alpha B_{lk}} \right)^T \dot{\hat{p}}_{ij}^{\alpha B_{lk}} \right] \}. \end{aligned} \quad (56)$$

Substituting (41) into (56), we have

$$\begin{aligned} \dot{L}(\hat{q}^\alpha, \hat{p}^\alpha) &= \sum_{l=1}^a \sum_{k=1}^b \left\{ - \sum_{i=1}^{n_l} \sum_{j=1}^{m_k} (\hat{p}_{ij}^{\alpha B_{lk}})^T \right. \\ &\quad \times \left[\sum_{N_{pq}^{\alpha B_{lk}}(t)} a_{ij,pq}(t) \cdot \hat{p}_{ij,pq}^{\alpha\alpha B_{lk}} + c_4 \hat{p}_{ij}^{\alpha B_{lk}} \right] \} \}. \end{aligned} \quad (57)$$

Using Lemma 1, (57) can be rewritten as

$$\dot{L}(\hat{\mathbf{q}}^\alpha, \hat{\mathbf{p}}^\alpha) = -(\hat{\mathbf{p}}^\alpha)^T [(\mathbf{L}(t) + c_4 I'_n) \otimes I_n] (\hat{\mathbf{p}}^\alpha) \quad (58)$$

where I'_n and I_n are identity matrices, and \otimes is the Kronecker product.

Considering \mathbf{L} to be a positive semidefinite matrix, thus, we have

$$-(\hat{\mathbf{p}}^\alpha)^T [(\mathbf{L}(t) + c_4 I'_n) \otimes I_n] (\hat{\mathbf{p}}^\alpha) \leq 0. \quad (59)$$

It follows from (59) that we have

$$\dot{L}(\hat{\mathbf{q}}^\alpha, \hat{\mathbf{p}}^\alpha) \leq 0. \quad (60)$$

Considering that the energy of swarm system is limited, it is easy to see

$$L(\hat{\mathbf{q}}^\alpha, \hat{\mathbf{p}}^\alpha) \leq L_0 \quad (61)$$

where L_0 is the initial energy of the swarm system, and $L_0 = C$.

Hence, the convergence of swarm system in Theorem 1 is proved.

B. Proof of Speed Consistency

We first show that the speeds of UAVs in the same group B_{lk} will eventually converge. Assuming that graph G is connected, there must be a connected path between the nodes ij and pq in graph G , whose length does not exceed $(n_l \times m_k - 1)$. In this way, we can obtain that the distance $\|\hat{\mathbf{q}}_{ij,pq}^{\alpha B_{lk}}\|_\sigma$ between UAV $\alpha_{ij}^{B_{lk}}$ and UAV $\alpha_{pq}^{B_{lk}}$ is bounded; the distance $\|\hat{\mathbf{q}}_{ij}^{\alpha B_{lk}}\|_\sigma$ between UAV $\alpha_{ij}^{B_{lk}}$ and the reference point of swarm structure is bounded, and their relative velocity in time $[t_d, t_{d+1}]$, ($d = 0, 1, \dots$) is also bounded. It follows that the point set $(\hat{\mathbf{q}}_{ij}^{\alpha B_{lk}}, \hat{\mathbf{p}}_{ij}^{\alpha B_{lk}})$ of UAV $\alpha_{ij}^{B_{lk}}$ is a compact set.

Combining Lemma 2 with (61), we can get that all UAVs in the same group will converge to the maximum invariant set, when the group system reaches a steady state, namely

$$S = \{(\hat{\mathbf{q}}^\alpha, \hat{\mathbf{p}}^\alpha) : -(\hat{\mathbf{p}}^\alpha)^T [(\mathbf{L}(t) + c_4 I'_n) \otimes I_n] (\hat{\mathbf{p}}^\alpha) = 0\}. \quad (62)$$

According to the property of the SOS of vectors, we can get

$$\hat{\mathbf{p}}^\alpha = 0. \quad (63)$$

Taking (38) into consideration, we get the speed of each UAV in one group as follows:

$$\mathbf{p}_{ij}^{\alpha B_{lk}} = \mathbf{p}^r. \quad (64)$$

The proof of speed consistency in one group is completed. Proceeding as in the proof of this, we get that the speeds of other groups of UAVs will eventually converge to the value of the maximum invariant set, namely

$$\mathbf{p}_{ij}^{\alpha B_{12}} = \mathbf{p}_{ij}^{\alpha B_{21}} = \dots = \mathbf{p}_{ij}^{\alpha B_{lk}} = \mathbf{p}^r \\ (l = 1, \dots, a; k = 1, \dots, b). \quad (65)$$

C. Proof of No Collision

Next, contradiction is used to prove that the UAVs in the swarm system will not collide with obstacles at any time. Suppose that at least one UAV $\alpha_{ij}^{B_{lk}}$ is colliding with an obstacle at time t_1 ($t_1 > 0$) in the swarm system. Combining the definition

of potential field function ψ^o in (29), we can obtain that the value of potential field ψ^o for UAV $\alpha_{ij}^{B_{lk}}$ tends to the infinite, namely

$$\psi^o \left(\left\| \mathbf{q}_{ij,\nu}^{\alpha o B_{lk}} \right\|_\sigma \right) \rightarrow \infty. \quad (66)$$

Substituting (66) into (51), we can obtain

$$L(\hat{\mathbf{q}}^\alpha, \hat{\mathbf{p}}^\alpha) \rightarrow \infty \quad (67)$$

which leads to a contradiction with (61).

Therefore, the above assumption does not hold, which implies that there exists no collision for UAV $\alpha_{ij}^{B_{lk}}$ with the obstacles during the flying process. As before, we identify the other group UAVs as obstacles. Hence the proof of no collision between UAVs is similar to the above proof, which is omitted here. Finally, we obtain that under the control law in (41), the swarm system can achieve obstacle avoidance and collision avoidance control.

REFERENCES

- [1] G. Skorobogatov, C. Barrado, and E. Salam, "Multiple UAV systems: A survey," *Unmanned Syst.*, vol. 8, no. 2, pp. 149–169, 2020.
- [2] J. Tang, S. Lao, and Y. Wan, "Systematic review of collision avoidance approaches for unmanned aerial vehicles," *IEEE Syst. J.*, vol. 16, no. 3, pp. 4356–4367, Sep. 2022.
- [3] B. K. Sahu and B. Subudhi, "Flocking control of multiple AUVs based on fuzzy potential functions," *IEEE Trans. Fuzzy Syst.*, vol. 26, no. 5, pp. 2539–2551, Oct. 2018.
- [4] H. Zhao, Y. Wen, S. Wu, and J. Deng, "Dynamic evaluation strategies for multiple aircrafts formation using collision and matching probabilities," *IEEE/CAA J. Automatica Sinica*, vol. 8, no. 4, pp. 890–904, Apr. 2021.
- [5] G. Jing and L. Wang, "Multiagent flocking with angle-based formation shape control," *IEEE Trans. Autom. Control*, vol. 65, no. 2, pp. 817–823, Feb. 2020.
- [6] X. Shao, Z. Cao, and H. Si, "Neurodynamic formation maneuvering control with modified prescribed performances for networked uncertain quadrotors," *IEEE Syst. J.*, vol. 15, no. 4, pp. 5255–5266, Dec. 2021.
- [7] J. Wu, H. Wang, N. Li, and Z. Su, "Formation obstacle avoidance: A fluid-based solution," *IEEE Syst. J.*, vol. 14, no. 1, pp. 1479–1490, Mar. 2020.
- [8] G. Lee and D. Chwa, "Decentralized behavior-based formation control of multiple robots considering obstacle avoidance," *Intell. Serv. Robot.*, vol. 11, no. 1, pp. 127–138, 2018.
- [9] D. Zhang, H. Duan, and Z. Zeng, "Leader–Follower interactive potential for target enclosing of perception-limited UAV groups," *IEEE Syst. J.*, vol. 16, no. 1, pp. 856–867, Mar. 2022.
- [10] X. Yan, D. Jiang, R. Miao, and Y. Li, "Formation control and obstacle avoidance algorithm of a multi-USV system based on virtual structure and artificial potential field," *J. Mar. Sci. Eng.*, vol. 9, no. 2, pp. 1–17, 2021.
- [11] S. Yang et al., "Neural-network-based formation control with collision, obstacle avoidance and connectivity maintenance for a class of second-order nonlinear multi-agent systems," *Neurocomputing*, vol. 439, pp. 243–255, 2021.
- [12] N. K. Long, K. Sammut, D. Sgarioto, M. Garratt, and H. A. Abbass, "A comprehensive review of shepherding as a bio-inspired swarm-robotics guidance approach," *IEEE Trans. Emerg. Topics Comput. Intell.*, vol. 4, no. 4, pp. 523–537, Aug. 2020.
- [13] S. Chen, H. Pei, Q. Lai, and H. Yan, "Multitarget tracking control for coupled heterogeneous inertial agents systems based on flocking behavior," *IEEE Trans. Syst. Man, Cybern. Syst.*, vol. 49, no. 12, pp. 2605–2611, Dec. 2019.
- [14] S. J. Chung, A. A. Paranjape, P. Dames, S. Shen, and V. Kumar, "A survey on aerial swarm robotics," *IEEE Trans. Robot.*, vol. 34, no. 4, pp. 837–855, Aug. 2018.
- [15] M. Waibel and F. Augugliaro, "Drone shows: Creative potential," Jan. 2017, [Online]. Available: www.veritystudios.com
- [16] X. Zheng et al., "Visually smooth multi-UAV formation transformation," *Graph. Models*, vol. 116, 2021, Art. no. 101111.
- [17] K. Kaplan, "500 drones light night sky to set record," IQ by Intel, Nov. 4, 2016, [Online]. Available: <https://iq.intel.com/500-drones-light-show-sets-record/>
- [18] Ehang, China. [Online]. Available: www.ehang.com/formation/
- [19] H. Rastgoftar and I. V. Kolmanovsky, "Safe affine transformation-based guidance of a large-scale multi-quadcopter system (MQS)," *IEEE Trans. Control Netw. Syst.*, vol. 8, no. 2, pp. 640–653, Jun. 2021.

- [20] J. Lwowski, A. Majumdar, P. Benavidez, J. J. Prevost, and M. Jamshidi, "Bird flocking inspired formation control for unmanned aerial vehicles using stereo camera," *IEEE Syst. J.*, vol. 13, no. 3, pp. 3580–3589, Sep. 2019.
- [21] L. Hong, H. Guo, J. Liu, and Y. Zhang, "Toward swarm coordination: Topology-aware Inter-UAV routing optimization," *IEEE Trans. Veh. Technol.*, vol. 69, no. 9, pp. 10177–10187, Sep. 2020.
- [22] "Department of defense announces successful micro-drone demonstration," U.S. Dept. Defense, Jan. 9, 2017, [Online]. Available: www.defense.gov/News/News-Releases/News-Release-View/Article/1044811/department-of-defense-announces-successful-microdrone-demonstration/
- [23] G. Vasarhelyi, C. Viragh, G. Somorjai, T. Nepusz, A. E. Eiben, and T. Vicsek, "Optimized flocking of autonomous drones in confined environments," *Sci. Robot.*, vol. 3, no. 20, 2018, Art. no. eaat3536.
- [24] X. Wang et al., "Coordinated flight control of miniature fixed-wing UAV swarms: Methods and experiments," *Sci. China Inf. Sci.*, vol. 62, no. 11, pp. 1–17, 2019.
- [25] H. Chen, X. Wang, L. Shen, and Y. Cong, "Formation flight of fixed-wing UAV swarms: A group-based hierarchical approach," *Chin. J. Aeronaut.*, vol. 34, no. 2, pp. 504–515, 2020.
- [26] T. H. Chung, M. R. Clement, M. A. Day, K. D. Jones, D. Davis, and M. Jones, "Live-fly, large-scale field experimentation for large numbers of fixed-wing UAVs," in *Proc. IEEE Int. Conf. Robot. Autom.*, 2016, pp. 1255–1262.
- [27] A. Kushleyev, D. Mellinger, C. Powers, and V. Kumar, "Towards a swarm of agile micro quadrotors," *Auton. Robots*, vol. 35, no. 4, pp. 287–300, 2013.
- [28] O. Holland and C. Melhuish, "Stigmergy, self-organization, and sorting in collective robotics," *Artif. Life*, vol. 5, no. 2, pp. 173–202, 1999.
- [29] Ö. Gürcan, "Proof of work is a stigmergic consensus algorithm: Unlocking its potential," *IEEE Robot. Autom. Mag.*, vol. 29, no. 2, pp. 21–32, Jun. 2022.
- [30] A. Kasprzok, B. Ayalew, and C. Lau, "An ant-inspired model for multiagent interaction networks without stigmergy," *Swarm Intell.*, vol. 12, no. 1, pp. 53–69, 2018.
- [31] Q. Tang, Z. Xu, F. Yu, Z. Zhang, and J. Zhang, "Dynamic target searching and tracking with swarm robots based on stigmergy mechanism," *Robot. Auton. Syst.*, vol. 120, 2019, Art. no. 103251.
- [32] P. Shi and B. Yan, "A survey on intelligent control for multiagent systems," *IEEE Trans. Syst. Man. Cybern. Syst.*, vol. 51, no. 1, pp. 161–175, Jan. 2021.
- [33] X. Dong, Y. Li, C. Lu, G. Hu, Q. Li, and Z. Ren, "Time-varying formation tracking for UAV swarm systems with switching directed topologies," *IEEE Trans. Neural Netw. Learn. Syst.*, vol. 30, no. 12, pp. 3674–3685, Dec. 2019.
- [34] T. Z. Muslimov and R. A. Munasypov, "Consensus-based cooperative control of parallel fixed-wing UAV formations via adaptive backstepping," *Aerospace Sci. Technol.*, vol. 109, 2021, Art. no. 106416.
- [35] J. Zhang and J. Yan, "A novel control approach for flight-stability of fixed-wing UAV formation with wind field," *IEEE Syst. J.*, vol. 15, no. 2, pp. 2098–2108, Jun. 2021.
- [36] M. A. Azam, H. D. Mittelmann, and S. Ragi, "UAV formation shape control via decentralized Markov decision processes," *Algorithms*, vol. 14, no. 3, pp. 1–12, 2021.
- [37] R. Wiltschko, K. Stapput, P. Thalau, and W. Wiltschko, "Directional orientation of birds by the magnetic field under different light conditions," *J. Roy. Soc. Interface*, vol. 7, no. suppl_2, pp. S163–S177, 2010.
- [38] R. Olfati-Saber, "Flocking for multi-agent dynamic systems: Algorithms and theory," *IEEE Trans. Autom. Control*, vol. 51, no. 3, pp. 401–420, Mar. 2006.
- [39] D. Shevitz and B. Paden, "Lyapunov stability theory of nonsmooth systems," *IEEE Trans. Autom. Control*, vol. 39, no. 9, pp. 1910–1914, Sep. 1994.



Jiacheng Li was born in Xining City, Qinghai Province, China, in 1997. He received the B.S. degree in automation from Nanjing Agricultural University, Nanjing, China, in 2020. He is currently working toward the M.S. degree with the Unmanned system Research Institute, Northwestern Polytechnical University, Xian, China.

His current research interests include collision avoidance control of UAV swarm, multiagent system control, and teleoperation control of unmanned driving robot.



Yangwang Fang was born in China in 1966. He received the Ph.D. degree in control science and engineering from Xian Jiaotong University, Xi'an, China, in 1998.

He is currently a Professor with Northwestern Polytechnical University, Xi'an, and an Adjunct Professor with Xian Jiaotong University and the Xian University of Electronic Science and Technology. He is also the Executive Director of Shaanxi Automation Society and Shanxi Signal Processing Society. His research interests include aircraft guidance and control, stochastic optimal control, nonlinear control, and intelligent information processing.



Haoyun Cheng received the B.S. degree in automation from Northwestern Polytechnical University, Xian, China, in 2011, and the Ph.D. degree in flight vehicle design from Beihang University, Beijing, China, in 2017.

He is currently an Assistant Professor with the Unmanned System Research Institute, Northwestern Polytechnical University, Xian, China. His current research interests include intelligent control, multi-aircraft cooperative guidance control, and intelligent aircraft design.



Zhikai Wang received the B.E. and M.Sc. degree in control science and engineering from the Henan University of Science and Technology, Luoyang, China, in 2016 and 2018, respectively. He is currently working toward the Ph.D. degree with the School of Aerospace, Northwestern Polytechnical University, Xian, China.

His current research interests include cooperative guidance, aircraft guidance and control, and path planning.



Zihao Wu was born in Lanzhou, China in 1992. He received the M.S. and Ph.D. degrees in aerospace control engineering from Northwestern Polytechnical University, Xi'an, China, in 2017 and 2022, respectively.

He is currently a Postdoctor with the Beijing University of Aeronautics and Astronautics, Beijing, China. At present, he has authored or coauthored some research results on the cooperative midcourse guidance of multiple missiles. His work focuses on cooperative guidance, aircraft or missile guidance and control, path planning.



Mengjie Zeng received the B.S. degree in automation from Nanjing Agricultural University, Nanjing, China. She is currently working toward the M.S. degree in mechanical with the Nanjing University of Aeronautics and Astronautics, Nanjing.

At present, she is mainly responsible for the fund projects related to intelligent diagnosis and also participates in the national key research and development program projects. Her main research fields include deep learning, intelligent fault diagnosis, and intelligent control theory and application.